



# Atomic Structure and Crystalline Order of Graphene-Supported Ir Nanoparticle Lattices

D. Franz,<sup>1,2,3</sup> S. Runte,<sup>4</sup> C. Busse,<sup>4</sup> S. Schumacher,<sup>4</sup> T. Gerber,<sup>4</sup> T. Michely,<sup>4</sup>  
M. Mantilla,<sup>5</sup> V. Kilic,<sup>1</sup> J. Zegenhagen,<sup>6</sup> and A. Stierle<sup>1,2,3,\*</sup>

<sup>1</sup>Universität Siegen, D-57072 Siegen, Germany

<sup>2</sup>Deutsches Elektronen-Synchrotron DESY, D-22603 Hamburg, Germany

<sup>3</sup>Fachbereich Physik, Universität Hamburg, D-20355 Hamburg, Germany

<sup>4</sup>Universität zu Köln, D-50937 Köln, Germany

<sup>5</sup>Max-Planck-Institut für autonome Systeme, D-70569 Stuttgart, Germany

<sup>6</sup>European Synchrotron Radiation Facility, F-38043 Grenoble, France

(Received 25 June 2012)

**I** We present the atomic structure of Ir nanoparticles with a 1.5 nm diameter and three layers average height grown on graphene/Ir(111). Using surface x-ray diffraction, we demonstrate that Ir nanoparticles on graphene/Ir(111) form a crystallographic superlattice with high perfection. The superlattice arrangement allows us to obtain detailed information on the atomic structure of the nanoparticles themselves, such as size, shape, internal layer stacking and strain. Our experiments disclose that the nanoparticles reside epitaxially on top of the graphene moiré structure on Ir(111), resulting in significant lateral compressive intraparticle strain. Normal incidence x-ray standing wave experiments deliver additional information on the particle formation induced restructuring of the graphene layer.

DOI:

PACS numbers: 61.48.Gh, 61.05.cf, 61.46.Df, 68.49.Uv

Ultrasmall metallic nanoparticles exhibit altered structural, chemical and magnetic properties as compared to their bulk counterparts making them attractive for applications as highly active heterogeneous catalysts or high storage density magnetic media [1–3]. To pinpoint structure-functionality relationships for systems containing nanoparticles with diameters smaller than 2 nm an atomic scale understanding of their structure is mandatory. However, for such small nanoobjects the atomic scale characterization by diffraction, x-ray absorption spectroscopy or electron microscopy is a tremendous challenge [4], additionally complicated by random nanoparticle orientation, large size and shape variations as well as by low particle concentration. X-ray powder diffraction and the corresponding pair distribution function analysis suffer from a pronounced particle size broadening and overlapping of Bragg reflections. Further on, the detailed structural investigation of supported nanoparticles by surface sensitive methods like scanning tunneling microscopy is hampered by the intrinsic high surface corrugation.

**7** As we will demonstrate in this Letter, the atomic scale determination of the internal nanoparticle structure with high crystallographic precision becomes feasible by surface x-ray diffraction (SXR) employing a trick. We use a two dimensional template, graphene on a Ir(111) surface, producing a regular arrangement of nanoparticles in the size regime below 2 nm by epitaxial growth. The nanoparticles act in this case as a two-dimensional optical grating for x-rays resulting in superlattice Bragg rods. These are modulated by the average three-dimensional structure factor of the individual nanoparticles, disclosing information on their internal structure, following one of the

basic principles of x-ray diffraction from crystals [5]. Complementary information on nanoparticle adsorption induced changes of the graphene layer structure was obtained by normal incidence x-ray standing wave (NIXSW) experiments.

Recently, it was demonstrated that Ir or Ru supported graphene acts as a template for the tailored growth of 4d and 5d transition metal nanoparticles in the form of highly ordered, hexagonal arrays adopting the graphene moiré unit cell of  $2.5 \times 2.5 \text{ nm}^2$  [6–10]. Because of their narrow particle size and distance distribution such systems may be regarded as very promising model systems for the investigation of heterogeneous catalytic reactions or nanoscale magnetism but important aspects of the atomic structure such as epitaxy to the underlying graphene/Ir support, as well as intraparticle strain, angular particle misorientation or the presence of intraparticle defects remain to be uncovered. As we demonstrate here, Ir nanoparticles on graphene/Ir(111) form a long range ordered crystalline superlattice not yet reported for nanoparticles grown on other templates such as the BN nanomesh [11] or Al<sub>2</sub>O<sub>3</sub> on Ni<sub>3</sub>Al(111) [12]. The system represents therefore an ideal showcase for the demonstration of our approach.

Prior to the x-ray experiments a clean Ir(111) surface was prepared by cycles of Ar ion sputtering and annealing up to 1450 K under ultra high vacuum (UHV). Graphene with high structural perfection was grown using ethylene as a carbon source (SXR: full layer, NIXSW: 0.6 ML) [13]. The graphene covered sample was mounted into a UHV x-ray diffraction chamber equipped with a sample heater and an Ir e-beam evaporator. In this case the graphene layer was cleaned from possible adsorbates by

flashing to 1220 K. For the NIXSW experiments graphene was grown *in situ* prior to the Ir deposition. In both cases Ir evaporation took place under UHV conditions, while the sample temperature was kept at 300 K, confining the growth of Ir nanoparticles to the graphene moiré unit cell [6]. The SXRD data were collected in  $z$ -axis geometry at the MPG beam line at the Ångströmquelle Karlsruhe (Germany) at a photon energy of 10 keV [14]. The x-ray structure factors were obtained by the integration of rocking scans around the surface normal and application of standard correction factors [15]. The fit of the x-ray data was performed using the software package ROD [16]. The NIXSW experiments were performed at the ESRF, Grenoble (France), beam line ID32 [17]. The standing wave was excited using the Ir(111) reflection at an incident photon energy of 2801 eV.

For the description of real and reciprocal space we employed a  $(9 \times 9)$  unit cell of the Ir(111) surface with  $a = b = 24.432 \text{ \AA}$ ,  $c = 6.650 \text{ \AA}$ ,  $\alpha = \beta = 90^\circ$ ,  $\gamma = 120^\circ$ . The graphene layer can be described in good approximation as a  $(10 \times 10)$  moiré structure coinciding with the  $(9 \times 9)$  unit cell on Ir(111) [6]. The reciprocal lattice is plotted in Fig. 1(a) and 1(b) together with a low energy electron diffraction (LEED) pattern of the pristine graphene layer after growth.

As a reference, we recorded the x-ray diffraction pattern of the pristine graphene layer. Figure 1(c) shows the  $(H = 0, K, L)$  plane, disclosing a rod like diffraction signal at  $K = 10$ , which is expected for a two-dimensional layer. The diffraction signal changes dramatically after deposition of  $(1.0 \pm 0.1)$  Ir(111) monolayer equivalent (ML): additional satellite rods are now detectable at the moiré reciprocal lattice positions  $(0,8)$  and  $(0,11)$  as well as at a variety of different  $(H, K)$  values, see Fig. 1(a). This observation is inline with the formation of a well-defined, coherent, epitaxial (111) oriented nanoparticle superlattice with the initial moiré period [18]. Further on, the intensity along the superstructure rods is modulated as a function of  $L$ , containing information on the three-dimensional structure of the nanoparticles. Remarkably, Debye-Scherrer rings from randomly oriented particles are absent.

Auxiliary information comes from  $K$  scans performed at  $(H = 0, L = 0.85)$ , plotted in Fig. 1(d): the maximum of the envelop function of the satellite peaks (labeled  $-1$ ,  $+1$ ,  $+2$ ) is shifted to higher momentum transfers  $Q$ , which gives direct evidence for a compression of the Ir nanoparticle in-plane atomic spacing [18]. From the resolution corrected in-plane width of the satellite reflections at  $(0,8)$  a coherent domain size of  $\approx 300 \text{ \AA}$  or 10 superstructure unit cells is deduced, which is identical to the initial structural coherence of the pristine graphene layer obtained from the graphene reflection at  $(0,10)$ . In addition, a broad diffraction signal is observed in the  $K$  scan after Ir deposition, which indicates that a non-negligible number of nanoparticles is uncorrelated and loses the stringent

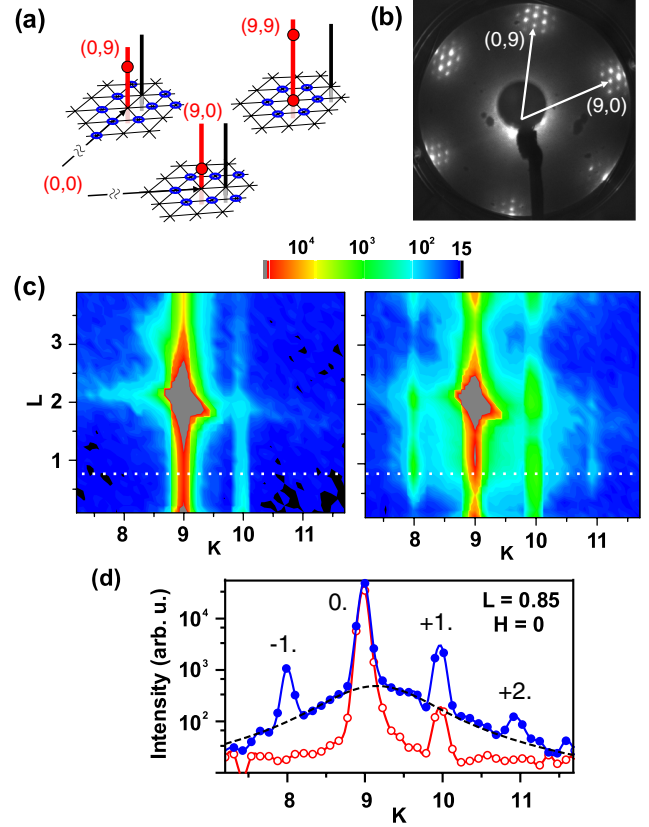


FIG. 1 (color online). (a) Reciprocal lattice sketch: thick (red) lines: crystal truncation rods (CTRs) from the Ir substrate (bulk Bragg reflections are indicated by closed circles), thin (black) lines: graphene rods, (blue) ellipses: reciprocal lattice positions, where additional reflections were observed after Ir deposition. (b) LEED pattern at 65 eV from the pristine graphene layer. (c) reciprocal space map of the  $(H = 0, K, L)$  plane before (left) and after (right) Ir deposition. (d)  $K$  scans at  $L = 0.85$  along the dashed lines in (c). (Red) open circles: before Ir deposition, (blue) filled circles: after Ir deposition. The dashed line is a fit of the broad component (see text).

registry discussed above. From the fit of the broad component [dashed line in Fig. 1(d)] an average particle diameter of  $1.9 \pm 0.2 \text{ nm}$  and a contraction of the in-plane lattice spacing by 1.9% is determined.

To obtain quantitative information on the highly correlated nanoparticles' internal structure, a set of x-ray structure factors was collected, presented in Fig. 2, which may be grouped in the following way: the first three rows in Fig. 2 disclose surface rods only detectable after Ir deposition (group I); they provide mainly information on the nanoparticle internal structure. In row 4 data obtained at graphene rod positions are presented (group II), sensitive to the interface between the graphene layer and the Ir nanoparticles. The third data group (last row in Fig. 2) includes crystal truncation rod (CTR) data from the Ir substrate which give information on the registry and distance of the particles with respect to the substrate.

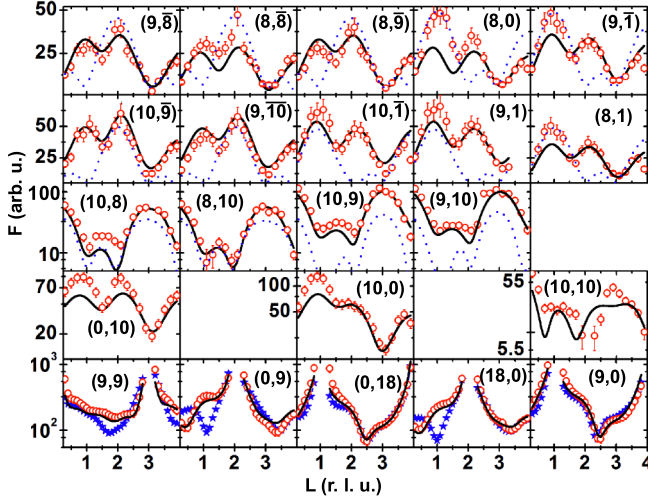


FIG. 2 (color online). Experimental x-ray structure factor magnitudes (open circles) together with error bars. The solid and dashed lines represent fits to the data and model calculations, respectively, as discussed in the text.

For the initial fit the shape and size of (111) oriented nanoparticles was varied using data group I. The best fit was achieved for three layers high, fcc particles containing 82 atoms with a hexagonal basis and a side length of four atoms, exhibits nanosized (100) and (111) type facets (see Fig. 3). The corresponding structure factors are plotted in

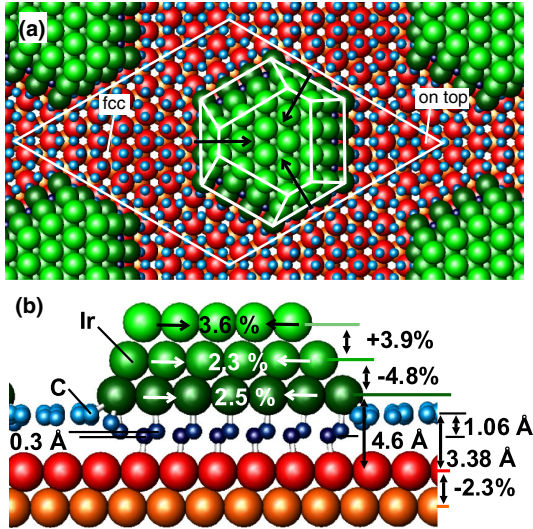


FIG. 3 (color online). (a) Top view of the structural model, the moiré unit cell is indicated by the white line. High symmetry sites are marked, where the center of the carbon rings is located either at a fcc or on-top site with respect to the substrate. The center of the nanoparticles is located at the hcp position of the carbon rings. The *ACB* stacked particles are rotated by  $60^\circ$  with respect to the *ABC* stacked particles (not shown). (b) Cross-sectional side view of the particles together with relaxation values. Not all C atoms are shown for clarity. The Ir(111) bulk layer spacing is  $2.216\text{\AA}$ .

Fig. 2, rows 1-3 as dashed lines for particles exhibiting the same “*ABC*” stacking as the bulk Ir crystal below, indicating that such a model reproduces only partially the data ( $\chi^2 = 10$ ) [16]. Statistical inclusion of particles with inverted “*ACB*” stacking residing at the same position inside the unit cell as the *ABC* stacked particles (equal probability within  $\pm 1.5\%$ ) leads to a much better agreement with the data ( $\chi^2 = 6$ ). For such unstrained particles, the satellite rod intensity is symmetric around the central Ir Bragg reflection, which is in contrast to the experimental observation [see Fig. 1(d)]. In the next step of the fit a centrosymmetric lateral “breathing” of the particles was introduced for each layer as indicated by the arrows in Fig. 3(a), resulting in an in plane reduction of the Ir-Ir distances by 2.5%, 2.3%, and 3.6% from the bottom to the top of the particles after the final refinement. The distance between the first and the second intraparticle Ir layer is found to be reduced by 4.8%, whereas the distance between the second and the third layer is expanded by 3.9%, likely induced by the strong in-plane contraction of the third layer.

Further on, the adsorption site of the particles with respect to the Ir(111) substrate and the  $z$  displacements were refined by a combined fitting of data group I and III, thereby keeping the center of the particles on a high symmetry “hcp” position with respect to the substrate. The best fit was obtained for a distance of  $(4.6 \pm 0.15 \text{\AA})$  between the topmost Ir substrate layer and the bottom nanoparticle layer. In a hard sphere model this distance gives room for a buckling of the graphene layer of about  $0.3 \text{\AA}$  below the Ir nanoparticles. This is inline with a diamond like structure at the interface as put forward recently based on density functional theory calculations [19], in which one half of the C atoms close to the hcp position in the unit cell sits directly below Ir atoms in the nanoparticles and the other half above Ir substrate atoms. Particles centered at the “fcc” position of the moiré unit cell give rise to a significantly worse fit, as indicated by the stars in the CTR data (last row in Fig. 2) and can therefore be ruled out by our experiments.

In addition, the fit of data group I and III yields occupation probabilities of the individual layers inside the nanoparticles delivering information on the statistical occupation of the moiré unit cells by coherently scattering nanoparticles (average layer occupation) and particle height distributions (differences in the occupation of the individual layers). We find the following occupancies: 53% of 37 atoms (1.layer), 49% of 27 atoms (2.layer), 45% of 18 atoms (3.layer). The fit is slightly improved by the inclusion of a 4.layer (12% occupancy of 10 atoms), corresponding in total to 42 Ir atoms [0.52 Ir (111) ML’s]. The result shows that 53% of the moiré unit cells are occupied by coherently scattering nanoparticles; the variation in occupation of the different layers translates into a height distribution of 6% for one layer, 9% for two layers, 63% for

three layers, and 22% for four layers high, agreeing well with scanning tunneling microscopy data [7]. As discussed above, about 24% of the particles are not in exact registry with the graphene/Ir(111) template. The missing fraction of 23% (1 monolayer deposited) indicates that for all particles a source of incoherency exists as may be represented by dynamical rotational fluctuations.

To gather additional structural information on the graphene layer after nanoparticle deposition, we performed XSW experiments near normal incidence. In Fig. 4 the C 1s photoemission signal is plotted as a function of the relative energy around the Ir(111) Bragg reflection before and after  $(0.9 \pm 0.2)$  ML Ir deposition on a Ir(111) surface covered by 0.6 ML graphene. The result of an XSW experiment, the coherent position  $P^H$  and the coherent fraction  $F^H$ , are determined by a fit to the data [20]. They roughly correspond to the mean adsorbate height and the distribution around this value [20]. The coherent position  $P^H$  of the graphene layer stays constant at  $(0.52 \pm 0.02)$  after Ir deposition and the coherent fraction  $F^H$  decreases to  $(0.33 \pm 0.04)$  compared to  $(0.74 \pm 0.04)$  for the pristine graphene layer [20,21]. The unchanged value of  $P^H$  and the reduction in  $F^H$  implies that there is a net increase in corrugation of the graphene layer after cluster deposition. Because of the expected large variation of the C atom heights the direct interpretation of  $P^H$  and  $F^H$  needs to be given up; specific combinations of  $P^H$  and  $F^H$  may, however, serve as a fingerprint for the correct graphene structure.

In the search for an adopted structural model of the graphene layer, we took an  $sp^3$  hybridized interfacial area with 74 C atoms into account, corresponding to one C atom per Ir atom of the first Ir layer of the nanoparticles

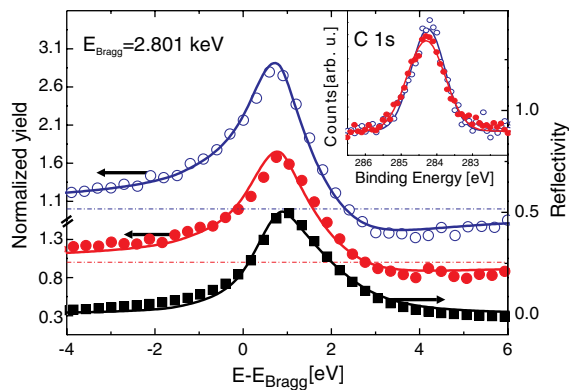


FIG. 4 (color online). C 1s XSW photoelectron yields of 0.63 ML C/Ir(111) normalized to the yield without Bragg reflected beam (dashed lines). Open circles: pristine graphene; filled circles: graphene +0.9 ML Ir; squares: normalized reflectivity. The curves are shifted for clarity. Solid lines represent fits to the data. Inset: C 1s core level line. Before (after) Ir deposition: open (filled) circles, respectively. Solid lines: fit with one Gaussian, Shirley background subtracted.

(37 atoms). We varied the structure of the pristine graphene layer using a simple Keating potential for the C-C interaction until we found  $P^H$  and  $F^H$  values close to the NIXSW results (0.51 and 0.29, respectively). The result is an egg box model similar to the one proposed for Pt on graphene/Ir(111) [22]; see Fig. 3(b). Using this interfacial model all diffraction data were fitted showing also good agreement for data group II ( $\chi^2 = 2.73$ ). A more elaborate structural analysis of the graphene layer is beyond the scope of the work presented here and would require a much larger data set. The nanoparticle induced increased modulation amplitude of the graphene layer is inline with previous density functional theory calculations on the adsorption of small Ir clusters (up to 19 atoms) [19]. In this study the average distance between a 19 atom Ir cluster and the first Ir substrate layer is calculated to be 4.61 Å, which matches very well to our experimental value of 4.6 Å. From our SXRD experiments we conclude that the carbon hybridization mediated bonding mechanism works even for larger islands with 37 atoms at the interface and that it is likely at the heart of the observed crystallographic nanoparticle superlattice arrangement.

Our analysis gives direct evidence for a contraction of the nanoparticle in-plane interatomic distances by 2.7% on average, which is significantly larger than reported for carbon supported Pt particles of similar size (0.5%) [23,24]. Such a variation in interatomic distances is expected to have an important impact on the catalytic activity of nanomaterials [25]. The observed contraction is on the one hand induced by the large atomic surface to volume ratio of 51:31 atoms. On the other hand, compressive epitaxial strain at the nanoparticle-graphene interface may play an important role since the lateral distance of the  $sp^3$  bonded carbon atoms at the interface is 2.58 Å matching well to the distance between Ir nearest neighbors in the first NP Ir layer (2.65 Å).

In conclusion, we have demonstrated that the atomic structure of Ir nanoparticles on graphene/Ir(111) with only 1.5 nm in diameter can be determined with atomic resolution, employing x-ray superlattice interferences. Because of the similarity in the bonding mechanism of overlapping  $5d$  and  $2p$  orbitals, we expect that Pt nanoparticles grown on graphene/Ir(111) with similar perfection, as well as other materials grown by Ir seeding such as Fe [7]. Our approach allows a direct correlation of the nanoparticles' atomic structure with catalytic activity or magnetic properties. The structural perfection of the particle superlattice is expected in turn to have dramatic consequences for the nanoparticle electronic structure such as zone folding and minigap formation.

Financial support by BMBF (Project No. 05K10PS1 “NanoXcat”) and DFG (MI517/17-2, BU2197/2-1) is gratefully acknowledged. The authors thank J. Coraux and R. Djemour for their help with the XSW data analysis.

\*Corresponding author.  
andreas.stierle@desy.de

- 2**  
**3**
- [1] S. N. Khanna and A. W. Castleman, *Quantum Phenomena in Clusters and Nanostructures* (Springer, Berlin, 2003).
- [2] U. Heiz and U. Landmann, *Nanocatalysis* (Springer, Berlin, 2006).
- [3] G. Ertl, H. Knözinger, F. Schüth, and J. Weitkamp, *Handbook of Heterogeneous Catalysis* (Wiley-VCH, Weinheim, Germany, 2008).
- [4] S. J. L. Billinge, I. Levin, *Science* **316**, 27 (2007).
- [5] B. E. Warren, *X-ray Diffraction* (Dover, New York, 1990).
- [6] A. T. N'Diaye, S. Bleikamp, P. J. Feibelman, and T. Michely, *Phys. Rev. Lett.* **97**, 215501 (2006).
- [7] A. T. N'Diaye, T. Gerber, C. Busse, J. Myslivecek, J. Coraux, and T. Michely, *New J. Phys.* **11**, 103045 (2009).
- [8] K. Donner and P. Jakob, *J. Chem. Phys.* **131**, 164701 (2009).
- [9] Q. Liao, H. J. Zhang, K. Wu, H. Y. Li, S. N. Bao, and P. He, *Nanotechnology* **22**, 125303 (2011).
- 4**
- [10] E. Sutter, P. Albrecht, B. Wang, M.-L. Bocquet, L. Wu, Y. Zhu, and P. Sutter, *Surf. Sci.* **605**, 1676 (2011).
- [11] M. L. Ng, A. B. Preobrajenski, A. S. Vinogradov, and N. Mårtensson, *Surf. Sci.* **602**, 1250 (2008).
- [12] A. Buchsbaum, M. De Santis, H. C. N. Tolentino, M. Schmid, and P. Varga, *Phys. Rev. B* **81**, 115420 (2010).
- [13] R. van Gastel, A. T. N'Diaye, D. Wall, J. Coraux, C. Busse, N. M. Buckanie, F.-J. Meyer zu Heringdorf, M. Horn von Hoegen, T. Michely, and B. Poelsema, *Appl. Phys. Lett.* **95**, 121901 (2009).
- [14] A. Stierle, A. Steinhauser, A. Ruhm, F. U. Renner, R. Weigel, N. Kasper, and H. Dosch, *Rev. Sci. Instrum.* **75**, 125302 (2004).
- [15] E. Vlieg, *J. Appl. Crystallogr.* **30**, 532 (1997).
- [16] E. Vlieg, *J. Appl. Crystallogr.* **33**, 401 (2000).
- [17] J. Zegenhagen, B. Detlefs, T.-L. Lee, S. Thiess, H. Isern, L. Petit, L. André, J. Roy, Y. Mi, and I. Joumard, *J. Electron Spectrosc. Relat. Phenom.* **178–179**, 258 (2010).
- [18] U. Pietsch, V. Holy, T. Baumbach, *High-Resolution X-Ray Scattering* (Springer, Berlin, 2004).
- [19] P. J. Feibelman, *Phys. Rev. B* **77**, 165419 (2008).
- [20] J. Zegenhagen, *Surf. Sci. Rep.* **18**, 199 (1993).
- [21] C. Busse *et al.*, *Phys. Rev. Lett.* **107**, 036101 (2011).
- [22] J. Knudsen, P. Feibelman, T. Gerber, E. Grånäs, K. Schulte, P. Stratmann, J. Andersen, and T. Michely, *Phys. Rev. B* **85**, 035407 (2012).
- [23] A. I. Frenkel, C. W. Hills, and R. G. Nuzzo, *J. Phys. Chem. B* **51**, 105 (2001).
- [24] For the incoherent particles with average size of 1.9 nm an in-plane contraction by 1.9% is observed, inline with the strain release by coalescence, which may set in at this particle size. **5**
- [25] M. Mavrikakis, B. Hammer, and J. K. Nørskov, *Phys. Rev. Lett.* **81**, 2819 (1998).
- [26] See Supplemental Material at <http://link.aps.org/supplemental/10.1103/PhysRevLett.000.000000> for [brief description]. **6**